Progress In Electromagnetics Research, Vol. 131, 227–241, 2012

AN ALTERNATIVE RANGE MIGRATION CORRECTION ALGORITHM FOR FOCUSING MOVING TARGETS

D. Kirkland*

Defence R & D Canada — Ottawa, 3701 Carling Ave., Ottawa, Ontario K1A0Z4, Canada

Abstract—This paper presents a method for focusing a moving target in single channel SAR data utilizing a novel technique for range migration correction. The First Order Keystone transform is first applied to remove the range-walk of the moving target signature. A search procedure based on maximizing a contrast cost function is then employed to determine the phase correction which compensates for the remaining range curvature. Finally an adaptive notch filter is used to construct an estimate of the azimuth compression filter necessary to focus the moving target. An experimental result is provided for airborne SAR data to demonstrate the feasibility of the approach.

1. INTRODUCTION

In a number of applications of Synthetic Aperture Radar (SAR) it is desirable to produce focused imagery of moving targets. SAR utilizes the known relative motion between the radar platform and the stationary background to produce high-resolution imagery. When a moving target is present in such an imaged scene it produces artifacts in the resulting SAR imagery. Velocity in the range direction produces additional range migration which results in a mis-positioning of the target in the azimuth direction with respect to the stationary background . Velocity in the azimuth direction or acceleration in the range direction results in a mismatch in the azimuth matched filter and produces smearing along the azimuth dimension in the SAR image. More detailed analysis of the effects of translational moving targets in SAR imagery appear in [1–4].

Focusing moving targets within SAR imagery requires the compensation of the range cell migration and the estimation of a

Received 7 June 2012, Accepted 29 August 2012, Scheduled 9 September 2012

* Corresponding author: David M. Kirkland (david.kirkland@drdc-rddc.gc.ca).

azimuth matched filter. Early techniques developed to address this problem assumed the range migration was negligible. Under this assumption the target energy is contained within a single range bin and traditional time-frequency techniques can be applied to construct the azimuth matched filter [5]. Unfortunately the constraint on the range migration limits these types of techniques to radar systems with low range resolution and low velocity targets.

Perry et al. [6] introduced the First-Order (Linear) Keystone transform, which is capable of removing the range walk component of the range migration of both stationary and moving targets simultaneously without a priori knowledge of the target velocity. To focus the moving target requires a search over a set of trial values which corrects the range curvature (quadratic) component of the range migration and performs azimuth compression. Since the azimuth filter is quite sensitive to this parameter, the search requires a finely spaced grid of trial values. The criterion for the search parameter was the maximization of the amplitude of one or more bright pixels in the corrected image.

Subsequently, the Second Order Keystone transform was introduced in [7]. This variation of the Keystone transform removes the range curvature of both the stationary and moving targets. A tracking approach was then utilized to estimate the range walk component of the moving target. The azimuth compression filter was determined by utilizing the Wigner-Ville (time-frequency) distribution. Another approach, based on the, Second Order Keystone transform, was presented in [8]. The principle of stationary phase was utilized to apply a Doppler Keystone transform (DKT) in the frequency-Doppler domain to remove the remaining range walk. azimuth compression was achieved using quadratic time-frequency distributions. These techniques have been demonstrated with point target responses but their effectiveness with more realistic target signatures remains to be seen.

In this paper, a novel approach is presented which addresses the range curvature and azimuth focusing issues encountered with the first order Keystone transform. After application of the Keystone transform a search procedure is used to apply a non-linear phase correction which compensates for the range curvature of the moving target. Unlike the approach in [6] the azimuth compression is avoided, which allows the search to take place over a coarser grid of trial values. The azimuth compression filter is generated by examining the parameters of an Adaptive Notch Filter (ANF) applied to the range migration corrected data. The ANF is capable of tracking the instantaneous frequency of the moving target signature which forms the basis for the azimuth

matched filter.

Section 2 reviews the Spotlight imaging geometry and develops the equation for the phase response of a moving target within the SAR data. Section 3 discusses the range migration correction procedure. Section 3.1 discusses the use of the Adaptive Notch Filter (ANF) for determination of the azimuth matched filter. Section 4 presents the results of the algorithm applied to airborne SAR data with a moving target.

2. SPOTLIGHT IMAGING GEOMETRY

The data collection geometry for the radar is shown in Fig. 1. For the purpose of consistency, this manuscript utilizes the same notation as [9]. The instantaneous radar position is given by $(0, u)$. X_c and Y_c denote the centre of the spotlight scene in the range and azimuth directions respectively. The instantaneous position of a moving target is given by $(X_c + x_0 + v_x u, Y_c + y_0 + v_y u)$, where x_0 and y_0 denote the initial offset position of the moving target from the scene centre in the range and azimuth directions respectively. v_x and v_y denote the moving target's velocities in the range and azimuth directions respectively. For convenience the velocity components of the moving target have been normalized by the radar platform velocity. After range compression and basebanding, the received radar signal for the

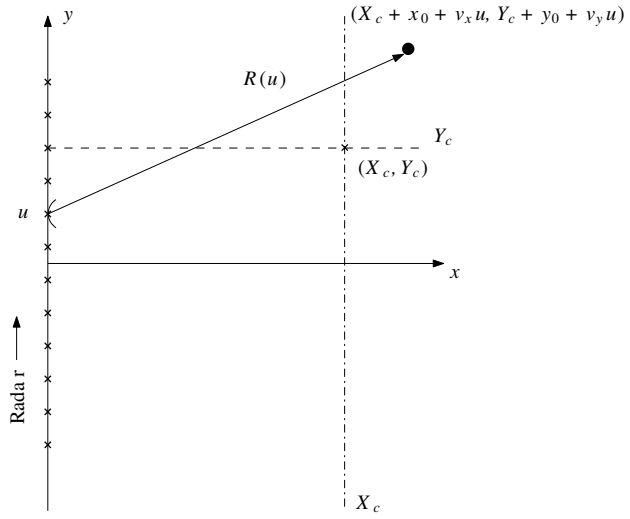

Figure 1. Imaging geometry.

moving target, $S(k,u)$, in the frequency-azimuth domain is:

$$S(k,u) = P(\omega)\exp\left(j\phi(k,u)\right), \tag{1}$$

where

$$\begin{aligned}
\phi(k,u) &= -2(k+k_0)R_\Delta(u), &(2)\\
R_\Delta(u) &= R(u) - R_{ref}(u), &(3)\\
R(u) &= \sqrt{(X_c+x_0+v_x u)^2+(Y_c+y_0+v_y u-u)^2}, &(4)
\end{aligned}$$

and

$$R_{ref}(u) = \sqrt{(X_c)^2+(Y_c-u)^2}. \tag{5}$$

$P(\omega)$ denotes the pulse response after range compression. k_0 is the wavenumber corresponding to the radar centre frequency. $k = \frac{\omega}{c}$ is the wavenumber (relative to k_0) in the fast time direction, and $\phi(k,u)$ denotes the phase response of the moving target.

In Appendix A, (A5) provides a general approximation for $R_\Delta(u)$ as:

$$R_\Delta(u) \approx \left(\cos\theta_c + \frac{\sin\theta_c\cos\theta_c}{R_c}u\right)(x_0+v_x u) + \left(\sin\theta_c - \frac{\cos^2\theta_c}{R_c}u\right)(y_0+v_y u), \tag{6}$$

where $\theta_c = \tan^{-1}(Y_c/X_c)$ denotes the squint angle when $u=0$. Squint mode operation and its effect on phase is described in [9] where it is shown that utilizing a rotated coordinate system can be used to reduce the squint mode case to a broadside geometry. For the remainder of this paper it is convenient to assume, without any loss of generality, that the radar operates around the point $\theta_c = 0$, i.e., broadside. This simplifies the subsequent mathematics, and (6) can then be written as

$$R_\Delta(u) = x_0 + \left(v_x - \frac{y_0}{R_c}\right)u - \frac{v_y}{R_c}u^2. \tag{7}$$

The phase response of the moving target is then obtained from (2) and (7) as

$$\phi(k,u) = -2(k+k_0)\left[x_0 + \left(v_x - \frac{y_0}{R_c}\right)u - \frac{v_y}{R_c}u^2\right]. \tag{8}$$

In (8) the phase terms dependent on k are responsible for the range migration effects, while the phase terms dependent on k_0 produce effects in the azimuth dimension such as azimuth translation and azimuth defocusing. Examination of the linear phase term w.r.t u in (8) reveals the velocity in the range direction corresponds to a displacement of the target signature in the cross-range direction of the SAR image. The presence of a cross range velocity produces a

quadratic term (w.r.t. u) in (8) and results in range curvature and smearing of the moving target signature in the cross-range direction in the resulting SAR image.

3. RANGE MIGRATION CORRECTION

To correct for the linear portion of the range migration, the First Order Keystone transform is first applied to (1), to give

$$S_k(k,u) = S\left(k, \left(\frac{k_0}{k+k_0}\right)u\right) = P(\omega)\exp(j\phi_k(k,u)). \tag{9}$$

The subscript k in both $S_k(k,u)$, and $\phi_k(k,u)$ is used to denote the signal components after application of the First Order Keystone transform. The resulting phase response is then given by

$$\begin{aligned}\phi_k(k,u) &= \phi\left(k, \left(\frac{k_0}{k+k_0}\right)u\right) \\ &= -2(k+k_0)x_0 - 2k_0\left(v_x - \frac{y_0}{R_c}\right)u + 2\frac{v_y}{R_c}\frac{k_0^2}{k+k_0}u^2. \end{aligned}\tag{10}$$

Due to the application of the dilation factor to the azimuth variable u, the quadratic term in u is non-linear with respect to frequency. Expanding (10) in a Taylor series w.r.t k about k_0 gives

$$\begin{aligned}\phi_k(k,u) \approx\ & -2(k+k_0)x_0 \\ & -2k_0\left(v_x - \frac{y_0}{R_c}\right)u + 2\frac{v_y}{R_c}(k_0-k)u^2. \end{aligned}\tag{11}$$

Examining (11) shows that the dominant impacts of the non-linear term are a azimuth chirp signal and the range curvature of the pulse envelope.

In [6], the full non-linear phase correction is applied, which corrects for range curvature and achieves azimuth compression. While the application of the proper phase correction will focus the moving target, it simultaneously defocuses the stationary clutter which makes the determination of the proper phase correction more difficult when the stationary clutter overlaps the moving target signature [2]. To alleviate this issue, the following phase correction is proposed in the current manuscript

$$\phi_{est}(k,u) = -2\frac{v_{y\_est}}{R_c}\frac{k_0^2}{k+k_0}u^2 + 2\frac{v_{y\_est}}{R_c}k_0u^2, \tag{12}$$

where v_{y_est} is an estimate of v_y. The phase correction in (12) is applied to (9) to give

$$\begin{aligned}S_c(k,u) &= S_k(k,u)\exp(j\phi_{est}(k,u)) \\ &= P(\omega)\exp(j\phi_c(k,u)). \end{aligned}\tag{13}$$

The subscript c is used in both $S_c(k,u)$, and $\phi_c(k,u)$ to denote the signal components after the proper phase correction is applied. The advantage of the phase correction in (12) is that it leaves the azimuth chirp of the moving target in the SAR data, and prevents the defocusing of the stationary targets.

The effectiveness of applying the phase correction $\phi_{est}(k,u)$ can be evaluated by utilizing a sharpness metric in the range-Doppler domain, i.e., $S_c(t,k_u)$. To determine the correct value of v_{y_est}, a discrete set of trial v_{y_est} values are applied and the value which maximizes sharpness metric given by

$$J(v_{y\_est}) = \sum_{t=t_{\min}}^{t_{\max}} \left(\sum_{k_u=-k_{\max}}^{k_{\max}} |S_c(t,k_u)| \right)^4, \tag{14}$$

is selected. In most SAR systems, there is a higher tolerance for error in the range migration correction than for the azimuth phase correction. Since the phase correction only needs to align the target energy within a single range bin, it does not need to be exact, and therefore a search can be performed over a much coarser grid than that of the algorithm given in [6].

Instead of a phase correction of the form of (12), it is possible to apply a correction based on linear or quadratic approximations to the phase correction, similar to that shown in (11). Unfortunately, the phase error with these approximations is directly proportional to u^2 and thus the error increases with the aperture length. Appendix B demonstrates the error in these types of approximations for both a high and a low frequency radar. The phase correction proposed in (12) avoids these types of errors and makes the algorithm applicable to a wider range of radar systems.

3.1. Azimuth Focusing

After application of the proper phase correction via (13), the phase response of the moving target is given by

$$\phi_c(k,u) = -2(k+k_0)x_0 - 2k_0\left(v_x - \frac{y_0}{R_c}\right)u + 2k_0\frac{v_y}{R_c}u^2. \tag{15}$$

A variety of techniques have been used to estimate the azimuth matched filter required to focus the moving target within the SAR image. Perry et al. [6] discuss a number of techniques based on the extraction of a strong point-like target. Non-parametric techniques based on the Wigner-Ville distribution were used in [5, 10, 11]. Another approach utilizes a high-order ambiguity function to estimate the

phase response of the moving target [12]. Unfortunately, many of these techniques work well under the assumption of a point-like target response, but their effectiveness on distributed targets has not yet been demonstrated.

A complex target, i.e., consisting of a set of point-like targets, with translational motion then each component of the target will produce a complex exponential having a phase similar to (15). Since the motion is translational, each exponential will have the same quadratic phase component due to the velocity v_y. If traditional quadratic time-frequency techniques are applied to estimate the phase of the overall target response, the estimate will suffer from cross term interference [13].

An alternative approach is to use an Adaptive Notch Filter (ANF) to track the quadratic component of the moving target response. The tracking performance of various ANF algorithms and structures has been extensively studied [14–17]. An additional benefit of the ANF approach is that it is capable of tracking higher order phase components which may be present due to the limitation of the Taylor series approximations or due to the presence of higher order translational motion terms, e.g., acceleration [3].

The ANF used in this algorithm is based on the constrained ANF structure developed by Nehorai [17]. The zero is constrained to be on the unit circle, and the pole is positioned in the same place as the zero, but is shifted radially inwards. The ANF is then given by

$$G(z) = \frac{A(z)}{A(\rho z)} = \frac{\left(1 - e^{j\theta} z^{-1}\right)}{\left(1 - \rho e^{j\theta} z^{-1}\right)}, \tag{16}$$

where ρ is the pole radius and is less than unity to ensure stability, and θ is the notch frequency. The filter bandwidth (BW) is given by:

$$BW = \pi(1 - \rho). \tag{17}$$

The Recursive Prediction Error (RPE) based algorithm derived in [18] is used to adaptively update the parameter θ.

If the pole of the ANF is close to the unit circle, the filter has a very narrow bandwidth. This provides a good estimate of the instantaneous frequency, but can prevent the filter from tracking the frequency changes. If the pole is shifted radially inwards the bandwidth of the filter is increased, but at the cost of increased variance of the frequency estimate [14–17]. In the algorithm presented in [18], the position of the pole is initially started to give the ANF a relatively large bandwidth to ensure the filter acquires the signal. The pole is then shifted radially towards the unit circle in a heuristic manner to reduce the filter bandwidth and reduce the variance of the frequency estimate. Further details are provided in [18].

The ANF is applied in the range-azimuth domain, i.e., $s_c(t,u)$, where $s_c(t,u)$ is the windowed inverse Fourier transform (IFT) of the phase corrected signal $S_c(t,k_u)$ taken in the azimuth direction. See Fig. 2. Utilizing a window to encompass the moving target signature prior to the IFT improves the signal to noise ratio (SNR) going into the ANF. The window is typically the same as the bins used for the evaluation of the phase correction applied in (14). The output of the ANF applied at the range bins corresponding to the target of interest is given by

$$s_n(t,u) = \rho e^{j\theta} s_n(t,u-1) + s_c(t,u) - e^{j\theta} s_c(t,u-1), \qquad (18)$$

where $s_n(t,u)$ represents the output of the ANF at azimuth position u.

Due to the closeness of the pole/zero pair in an ANF, the phase response of a non-adaptive filter is highly non-linear. For this reason the output of the ANF is not used directly to focus the moving target signature. Instead, the parameter θ, which is an estimate of the instantaneous frequency of the moving target, is integrated to generate the phase response of the matched filter. The phase of the azimuth matched filter, $\omega(t,u)$, can then be constructed for each range bin as

$$\omega(t,u) = \int_0^u \theta(t,u)du. \qquad (19)$$

A low order polynomial is used to approximate the estimated phase. The focussed image of the moving target can then be produced in the

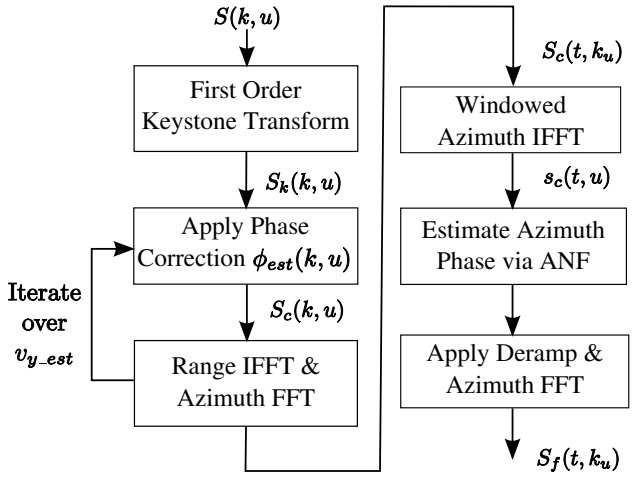

Figure 2. Algorithm flowchart for moving target imaging.

range-Doppler domain by using a deramping technique:

$$S_f(t, k_u) = \mathcal{F}_u[\exp(-j\omega_{poly}(t, u))s_c(t, u)], \tag{20}$$

where $\mathcal{F}_u$ denotes the Fourier transform in the azimuth direction and $\omega_{poly}(t, u)$ denotes the polynomial approximation to the phase $\omega(t, u)$.

It is important to note that the application of the matched filter for the moving target will result in the smearing of nearby stationary targets. Unfortunately there is currently no way of focusing stationary and moving targets simultaneously in single channel SAR systems.

4. RESULTS

In this section, experimental results demonstrating the effectiveness of the proposed algorithm are presented. The signal data were

Table 1. Data collection parameters.

Symbol	Description	Value
PRF	Pulse Repetition Frequency	1.0 kHz
R_0	range to scene centre	18.21 km
f_0	radar centre frequency	9.75 GHz
L	aperture length	407 m
θ_c	squint angle	24.74°
v_p	radar platform velocity	99 m/s
B_{az}	azimuth beamwidth	2.4°
Δr	range resolution	< 1 m

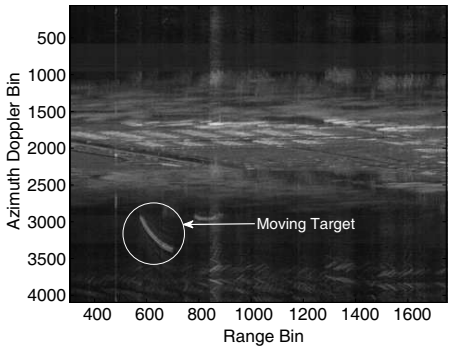

Figure 3. Full radar scene showing the moving target signature in the range-doppler domain.

collected with DRDC's X-band Wideband Experimental Airborne (XWEAR) system [19, 20]. The area imaged is the Connaught Range located near Ottawa, Canada. The dataset contains a moving target possessing a radial velocity, which is easily separable from the stationary background. This allows for the demonstration of the algorithm with a realistic moving target, and prevents the defocusing of the stationary data from masking the focused moving target. Table 1 shows the parameters of the radar and the data collection geometry.

Figure 3 shows the range compressed data in the range-Doppler domain. The signature of the moving target of interest is highlighted within the figure. Fig. 4 illustrates the effect of the various processing steps on the moving target signature in the range-Doppler domain.

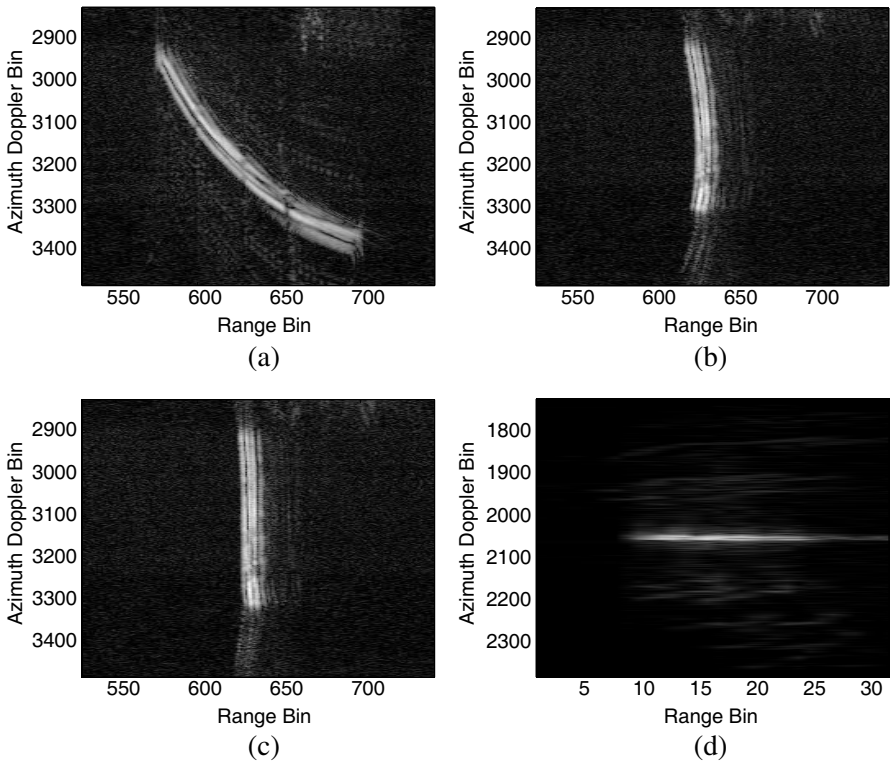

Figure 4. Images of the moving target (range-doppler) at various stages of the processing algorithm. (a) Moving target after range compression. (b) Moving target after first order keystone transform. (c) Moving target after range curvature correction. (d) Moving target after azimuth compression.

Fig. 4(a) shows the original moving target signature after range compression. Fig. 4(b) shows the result after application of the First Order Keystone transform and illustrates the reduction in range migration due to the elimination of range walk. In Fig. 4(c) shows the result after the phase correction has been applied to compensate for range curvature. At this point, the most significant portion of the range migration has been removed and the energy associated with the moving target signature is aligned along the range bins. Finally, the result after application of the azimuth matched filter, derived from the ANF, is shown in Fig. 4(d). Comparison of Fig. 4(c) and Fig. 4(d) demonstrates that significant azimuth compression has been achieved.

5. CONCLUSIONS

In this paper, an alternative algorithm for the correction of range migration associated with moving targets with a high azimuth velocity is presented. The First Order Keystone transform is applied to correct for range walk. A search procedure is used to determine the correct phase correction to compensate for range curvature. An adaptive IIR filter is then utilized to construct an azimuth compression filter. The effectiveness of the algorithm is demonstrated using data acquired with DRDC Ottawa's XWEAR system. Work is currently ongoing in extending this algorithm to focusing moving targets in multi-channel SAR data.

APPENDIX A. DERIVATION OF $R_\Delta(U)$ APPROXIMATION

The following derivation appears in [9] and is included here for completeness. In order to determine the effects of the First Order Keystone transform the phase in (1) needs to be expanded in a Taylor series in the azimuth direction. To simplify the calculation of the Taylor series, a binomial series expansion is first applied to $R_\Delta(u)$ w.r.t. the spatial variables x_0, v_x, y_0 and v_y. This leads to

$$R_\Delta(u) = \frac{X_c(x_0 + v_x u)}{R_{ref}(u)} + \frac{(Y_c - u)(y_0 + v_y u)}{R_{ref}(u)} + \dots. \tag{A1}$$

By ignoring higher order terms and defining the instantaneous squint angle $\theta(u) = \tan^{-1}\left(\frac{Y_c - u}{X_c}\right)$, (A1) can be written as

$$R_\Delta(u) = \cos\theta(u)(x_0 + v_x u) + \sin\theta(u)(y_0 + v_y u). \tag{A2}$$

Using a narrow beamwidth approximation, i.e., $u \ll \sqrt{X_c^2 + Y_c^2}$, $\theta(u)$ can be approximated by

$$\theta(u) \approx \theta_c - \frac{\cos\theta_c}{R_c} u, \tag{A3}$$

where $R_c = \sqrt{X_c^2 + Y_c^2}$ and $\theta_c = \theta(0)$. Applying standard trigonometric relationships leads to the following approximations

$$\begin{aligned} \sin\theta(u) &\approx \sin\theta_c - \frac{\cos^2\theta_c}{R_c} u, \\ \cos\theta(u) &\approx \cos\theta_c + \sin\theta_c \frac{\cos\theta_c}{R_c} u. \end{aligned} \tag{A4}$$

Substituting the approximations of (A4) in (A2) gives

$$R_\Delta(u) \approx \left(\cos\theta_c + \frac{\sin\theta_c \cos\theta_c}{R_c} u\right)(x_0 + v_x u) + \left(\sin\theta_c - \frac{\cos^2\theta_c}{R_c} u\right)(y_0 + v_y u). \tag{A5}$$

APPENDIX B. PHASE ERROR ANALYSIS

This section examines and quantifies the errors associated with using Taylor series approximations for the range curvature correction. Defining $\psi(k, u)$ as the nonlinear phase term responsible for the range curvature after applying the First Order Keystone transform gives

$$\psi(k, u) = 2\frac{v_y}{R_c} \frac{k_0^2}{k + k_0} u^2 \tag{B1}$$

Using a Taylor series expansion w.r.t. k about the point k_0, and keeping terms up to the quadratic gives

$$\psi(k, u) \approx 2\frac{v_y}{R_c} \left(k_0 - k + \frac{k^2}{k_0}\right) u^2 \tag{B2}$$

To demonstrate the magnitude of the phase errors associated with this approximation, consider two radar systems operating at $f_0 = 2.0\,\text{GHz}$ and $f_0 = 9.0\,\text{GHz}$. To simplify analysis, broadside operation for spotlight mode is assumed. If the radars are operating at a range of 20 km, and a azimuth resolution of 0.3 m is required, then the aperture length required at 2.0 GHz is approximately 5000 m (i.e., $-2500 < u < 2500$). Similarly an aperture length of approximately 1110 m is required at 9.0 GHz to achieve the 0.3 m resolution. To correspond to the 0.3 m azimuth resolution the pulse bandwidth is 500 MHz (i.e., $-5.236 \le k \le 5.236\,\text{rad/m}$).

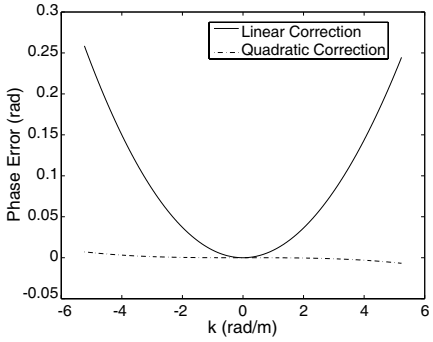

Figure B1. Phase error for linear and quadratic corrections. $f_0 = 9\,\text{GHz}$, $u = 555\,\text{m}$, $v_y = 0.056\,\text{m/s}$.

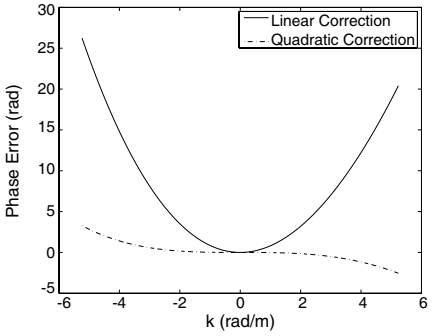

Figure B2. Phase error for linear and quadratic corrections. $f_0 = 2\,\text{GHz}$, $u = 2500\,\text{m}$, $v_y = 0.056\,\text{m/s}$.

Figure B1 illustrates the phase error for the linear and quadratic approximations at the extreme ends of the aperture for the high frequency radar. In the linear approximation the total error extent (max-min) is 0.26 rad, while for the quadratic approximation it is less than 0.015 rad. In both cases either approximation would not result in significant focusing artifacts, since they are less than the typical $\pi/2$ rad required for producing a focused image [21]. In contrast, Fig. B2 illustrates the error for the linear and quadratic approximations for the low frequency radar when $u = 2500$. In the linear approximation the total error extent is 26.2 rad. In the case of the quadratic approximation the total error extent is smaller, but still significant at 5.8 rad. At this frequency both of these approximations will result in significant focusing errors.

REFERENCES

1. Raney, R. K., "Synthetic aperture imaging radar and moving targets," *IEEE Transactions on Aerospace and Electronic Systems*, Vol. 7, No. 3, 499–505, May 1971.
2. Fienup, J., "Detecting moving targets in SAR imagery by focusing," *IEEE Transactions on Aerospace and Electronic Systems*, Vol. 37, No. 3, 794–808, Jul. 2001.
3. Sharma, J. J., C. H. Gierull, and M. J. Collins, "The influence of target acceleration on velocity estimation in dual-channel

SARGMTI," *IEEE Transactions on Geoscience and Remote Sensing*, Vol. 44, No. 1, 134–147, Jan. 2006.

4. Mao, X., D.-Y. Zhu, and Z.-D. Zhu, "Signatures of moving targets in polar format spotlight SAR image," *Progress In Electromagnetics Research*, Vol. 92, 47–64, 2009.
5. Barbarossa, S. and A. Farina, "Detection and imaging of moving objects with synthetic aperture radar — Part 2: Joint time frequency analysis by Wigner-Ville distribution," *IEE Proceedings — F*, Vol. 139, No. 1, 89–97, Feb. 1992.
6. Perry, R., R. DiPietro, and R. Fante, "SAR imaging of moving targets," *IEEE Transactions on Aerospace and Electronic Systems*, Vol. 35, No. 1, 188–200, Jan. 1999.
7. Zhou, F., R. Wu, and Z. Bao, "Approach for single channel SAR ground moving target imaging and motion parameter estimation," *IET Radar, Sonar, and Navigation*, Vol. 1, No. 1, 59–66, Feb. 2007.
8. Li, G., X.-G. Xia, and Y.-N. Peng, "Doppler keystone transform for SAR imaging of moving targets," *Congress on Image and Signal Processing*, 716–719, May 2008.
9. Kirkland, D., "Imaging moving targets using the second-order keystone transform," *IET Radar Sonar and Navigation*, Vol. 5, No. 8, 902–910, Oct. 2011.
10. Zhou, F., Y. Li, R. Ru, M. Xing, and Z. Bao, "An effective approach to ground moving target imaging for single channel SAR system," *International Conference on Radar*, 1–4, Oct. 2006.
11. Barbarossa, S. and A. Farina, "A novel procedure for detecting and focusing moving objects with SAR based on the Wigner-Ville distribution," *Record of the IEEE 1990 International Radar Conference*, 44–50, May 1990.
12. Barbarossa, S. and A. Scaglione, "Autofocusing of SAR images based on the product high-order ambiguity function," *IEE Proceedings Radar, Sonar, and Navigation*, Vol. 145, No. 5, 269–273, Oct. 1998.
13. Cohen, L., "Time-frequency distributions — A review," *Proceedings of the IEEE*, Vol. 77, No. 7, 941–981, Jul. 1989.
14. Rao, B. D. and R. Peng, "Tracking characteristics of the constrained IIR adaptive notch filter," *IEEE Transactions on Acoustics Speech and Signal Processing*, Vol. 36, No. 9, 1466–1479, Sep. 1988.
15. Regalia, P., *Adaptive IIR Filtering in Signal Processing and Control*, 1st edition, Marcel Dekker, Inc., Sep. 1994.

16. Händel, P. and A. Nehorai, "Tracking analysis of an adaptive notch filter with constrained poles and zeros," *IEEE Transactions on Signal Processing*, Vol. 42, No. 2, 281–291, Feb. 1994.
17. Nehorai, A., "A minimal parameter adaptive notch filter with constrained poles and zeros," *IEEE Transactions on Acoustics, Speech, and Signal Processing*, Vol. 33, No. 4, 983–996, Aug. 1985.
18. Pei, S.-C. and C.-C. Tseng, "Complex adaptive IIR notch filter algorithm and its applications," *IEEE Transactions on Circuits and Systems — II: Analog and Digital Signal Processing*, Vol. 41, No. 2, 158–163, Feb. 1994.
19. Damini, A., M. McDonald, and G. Haslam, "X-band wideband experimental airborne radar for SAR, GMTI and maritime surveillance," *IEE Proceedings Radar, Sonar and Navigation*, Vol. 150, No. 4, 305–312, Aug. 2003.
20. Damini, A., M. Balaji, L. Shafai, and G. Haslam, "Novel multiple phase centre reflector antenna for GMTI radar," *IEE Proceedings Microwaves, Antennas and Propagation*, Vol. 151, No. 3, 199–204, Jun. 2004.
21. Curlander, J. C. and R. N. McDonough, *Synthetic Aperture Radar Systems and Signal Processing*, 1st Edition, John Wiley & Sons, Inc., 1991.